Electronic Supplementary Material (ESI) for RSC Advances.

Supplementary Information

$Fe_2(MoO_4)_3$ nanoparticles-anchored MoO_3 nanowires: strong coupling via the reverse diffusion of heteroatoms and largely enhanced lithium-storage properties

Yeping Song [ab], Hai Wang *[ab], Zihua Li [a], Naiqing Ye [a] , Linjiang Wang [ab] and Yong Liu [c]

[a]College of Materials Science and Engineering, Guilin University of Technology, Guilin 541004, PR China

[b]Key Laboratory of New Processing Technology for Nonferrous Metals and Materials, Ministry of Education,Guilin University of Technology, Guilin 541004, PR China

Corresponding author E-mail address: hbwanghai@gmail.com (H. Wang).

Tel.: +86 773 5896672; fax: +86 773 5896671.

Figure captions

Fig.S1 TG-DSC pattern of MoO_3 nanobelts soaked in $FeCl_3$• $6H_2O$ via hydrothermal treatment at at 90 ℃ for 6 h.

Fig.S2 A typical TEM images of FM-600 (a)-(b), (c) HRTEM images of an individual nanoparticles composites and (d) the corresponding SAED. The two red arrow indicate some hollow hierarchical heterostructures.

Fig. S3 (a) STEM image of an individual FM-500 nanobelts and corresponding EDX elemental mapping of (b) Fe, (c) Mo and (d) O, respectively.

Scheme. S1. Schematic illustration of the morphology evolution process of MoO_3 nanobelts. (a) MoO_3 nanobelts; (b) FM-500 nanowires and (c) hollow hierarchical structural FM-600.

Fig. S4 The charge-discharge profiles of the MoO_3 nanobelts, FM-500, and FM-600 (a)-(c) and their corresponding dQ/dV profiles (d)-(f).

Fig. S5 The cycle performance of the MoO_3 nanobelts, FM-500 nanowires and FM-600 at 200 mA g^{-1}.

Fig. S6 Two typical HRTEM images of FM-500 nanowires (a)-(b), showing the location position relationship of MoO_3 nanobelts, $Fe_2(MoO_4)_3$ nanoparticles and amorphous layer.

Fig. S7. Nitrogen adsorption and desorption isotherms and pore-size distribution curves (inset) of the MoO_3 nanobelts (a), FM-500 nanowires (b), and MF-600 (c) sample. According to BJH method, a maximum of the pore size distribution taken from the description branch.

Fig. S8 The voltage profiles plotted for the first three charge-discharge cycles of the FM-500 nanobelts electrode at a current density of 100 mA g^{-1}.

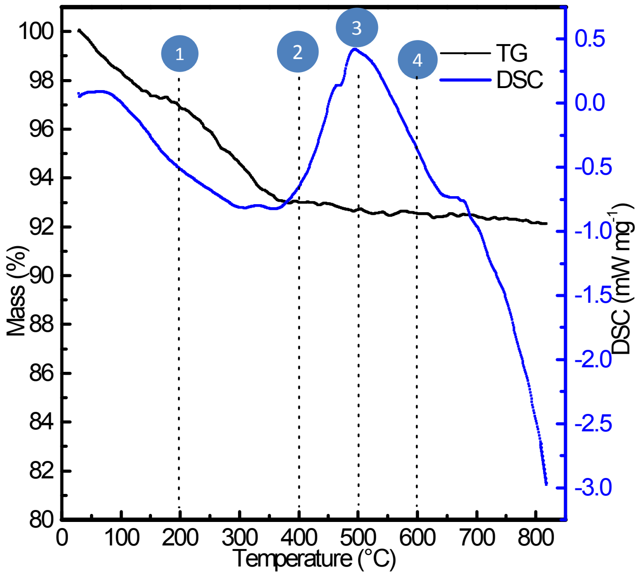

Fig. S1. TG-DSC pattern of MoO_3 nanobelts soaked in $FeCl_3$•$6H_2O$ via hydrothermal treatment at at 90 ℃ for 6 h.

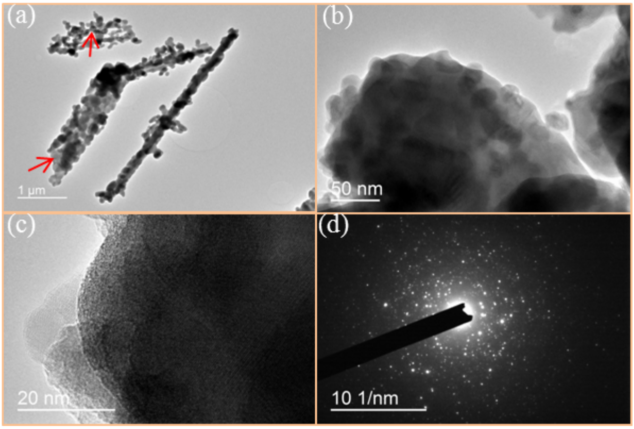

Fig.S2 A typical TEM images of FM-600 (a)-(b), (c) HRTEM images of an individual nanoparticles composites and (d) the corresponding SAED. The two red arrow indicate some hollow hierarchical heterostructures.

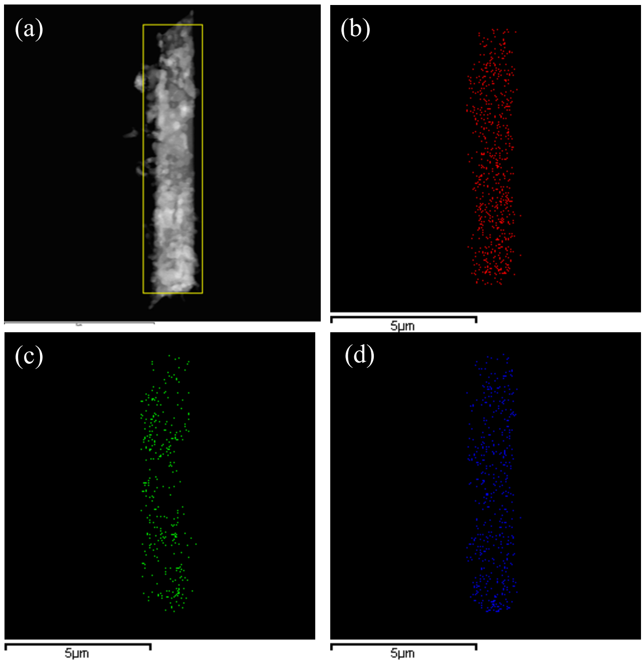

Fig. S3 (a) STEM image of an individual FM-500 nanobelts and corresponding EDX elemental mapping of (b) Fe, (c) Mo and (d) O, respectively.

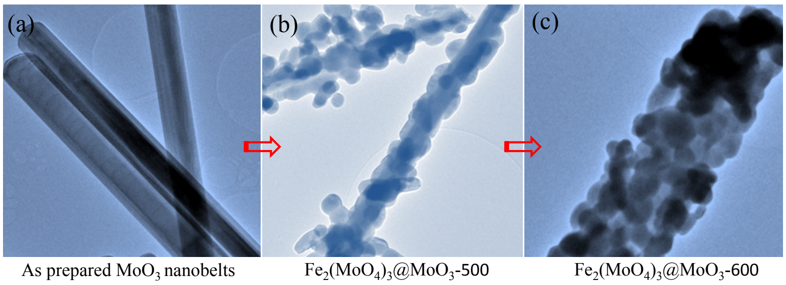

Scheme. S1. Schematic illustration of the morphology evolution process of MoO_3 nanobelts. (a) MoO_3 nanobelts; (b) FM-500 nanowires and (c) hollow hierarchical structural FM-600.

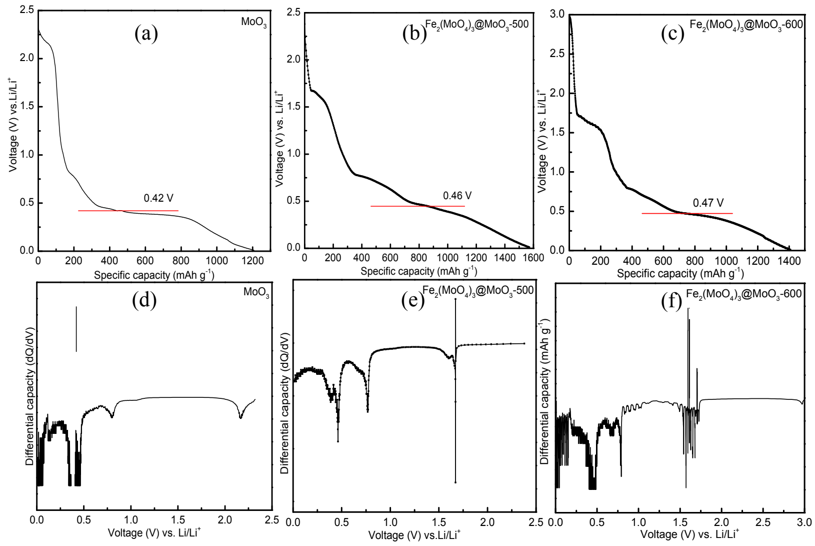

Fig. S4 The charge-discharge profiles of the MoO_3 nanobelts, FM-500, and FM-600 (a)-(c) and their corresponding dQ/dV profiles (d)-(f).

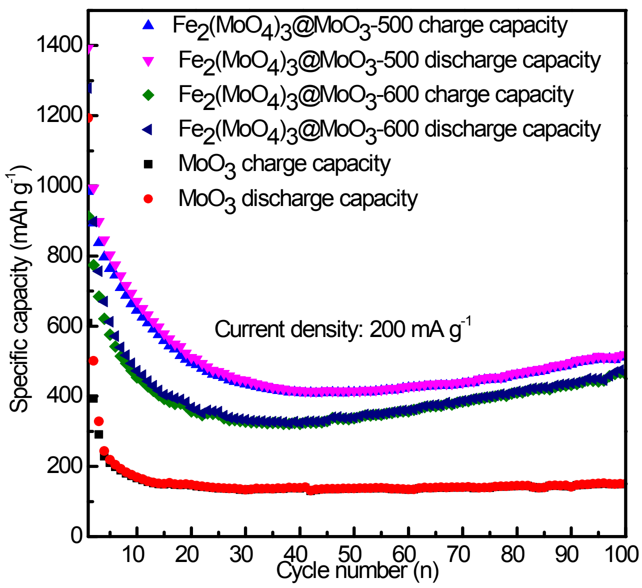

Fig. S5 The cycle performance of the MoO_3 nanobelts, FM-500 nanowires and FM-600 at 200 mA g^{-1}.

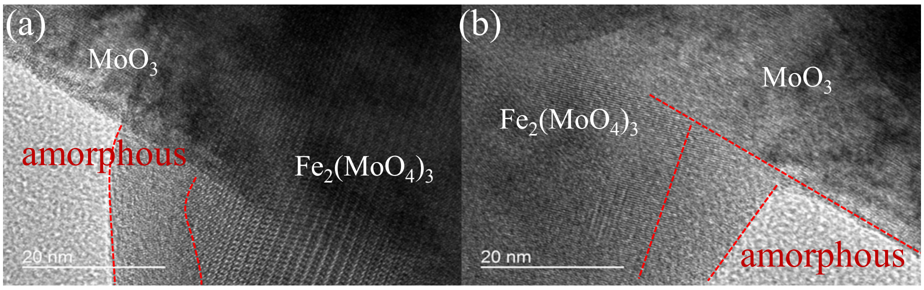

Fig. S6 Two typical HRTEM images of FM-500 nanowires (a)-(b), showing the location position relationship of MoO_3 nanobelts, $Fe_2(MoO_4)_3$ nanoparticles and amorphous layer.

The surface area and pore-size distribution are two key factors for active materials in electrochemical reaction; therefore, the surface area and porosity of the as-prepared samples were investigated by nitrogen sorption measurement (Fig. S7). As shown in Fig. S7, the isotherms of the three samples exhibit a typical mesoporous characteristic with distinct hysteresis. Moreover, the three samples exhibit a type IV isotherm as a result of the mesoporosity with an IUPAC type H3 hysteresis loop in the p/p_o range of 0.45-1.0 [1]. As listed in Tab. S1, the specific surface areas of MoO_3, FM-500 and FM-600 were determined to be 6.9, 22.5 and 13.38 m^2 g^{-1}, respectively. The increased specific surface area of FM-500 and FM-600 may be due to the mesoporous texture derived from the presence of the amorphous layer and the exposed $Fe_2(MoO_4)_3$ nanoparticles and the coarse of the surface of MoO_3 nanobelts.

The pore size distribution calculated from desorption data using the BJH model indicates that the pore size of the MoO_3 nanobelts, FM-500 nanowires and FM-600 sample appears to be primarily 9.04, 14.9 and 13.6 nm, respectively.

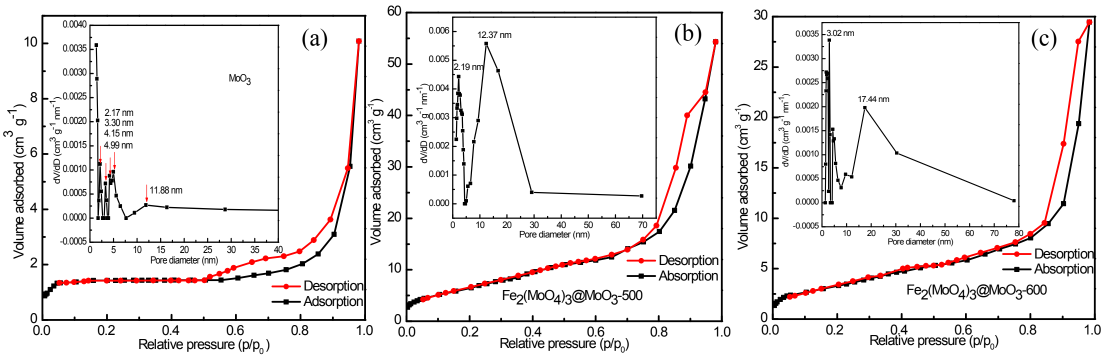

Fig. S7. Nitrogen adsorption and desorption isotherms and pore-size distribution curves (inset) of the MoO_3 nanobelts (a), FM-500 nanowires (b), and MF-600 (c) sample. According to BJH method, a maximum of the pore size distribution taken from the description branch.

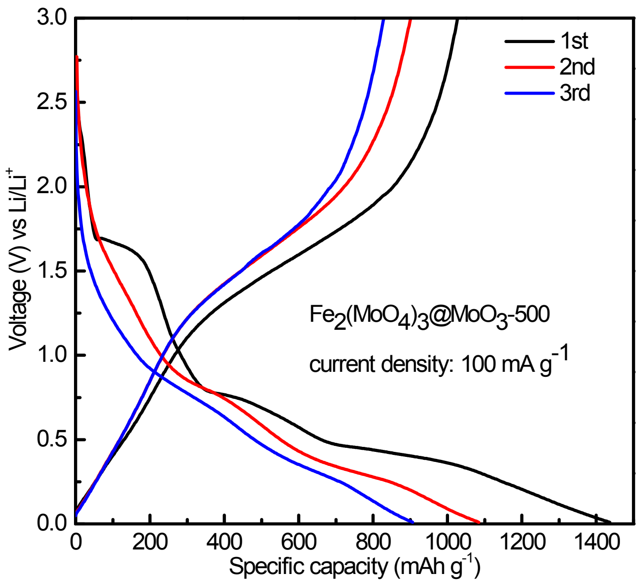

Fig. S8 The voltage profiles plotted for the first three charge-discharge cycles of the FM-500 nanobelts electrode at a current density of 100 mA g^{-1}.

Table captions

Tab. S1. Nitrogen physisorption parameters of the MoO_3 nanobelts, FM-500, and MF-600 samples.

Tab. S2 Impedance parameters of the MoO_3 nanobelts, FM-500, and MF-600 electrodes calculated from the equivalent circuit.

Tab. S1. Nitrogen physisorption parameters of the MoO_3 nanobelts, FM-500, and MF-600 samples.

Samples	Surface area [a] ($m^2\ g^{-1}$)	Pore volume [b] ($cm^3\ g^{-1}$)	Average pore diameter [c] (nm)
MoO_3	6.9	1.559×10^{-2}	9.04
FM-500	22.5	8.398×10^{-2}	14.9
FM-600	13.38	4.556×10^{-2}	13.6

[a]BET specific surface area calculated from the linear part of BET plot.

[b]Total pore volume taken from the volume of N_2 adsorbed at $p/p_0 = 0.98$.

[c]Average pore Radius was estimated from the Barrett-Joyner-Halenda formula.

Tab. S2 Impedance parameters of the MoO_3 nanobelts, FM-500, and MF-600 electrodes calculated from the equivalent circuit.

Electrode	R_s (Ω)	R_{ct} (Ω)	i^0 (mA cm^{-2})
MoO_3	2.25	245.5	0.017
FM-500	2.18	68.81	0.062
FM-600	4.11	128.7	0.033

References:

1. Gregg S J, Sing K S W. Adsorption, Surface Area, and Porosity. 1983